Structures and Properties of Newton Black Films Characterized Using Molecular Dynamics Simulations

Seung Soon Jang and William A. Goddard, III*

Materials and Process Simulation Center (MC 139-74) California Institute of Technology, Pasadena, California 91125

We used molecular dynamics (MD) simulations to investigate the structures and properties of Newton black films (NBF) for several surfactants: sodium dodecyl sulfate (SDS), cetyltrimethylammonium bromide (C16TAB), and surfactin using film thicknesses up to 10 nm. By calculating the interface formation energy for various packing conditions on the surface pressure−area isotherm, we found that the most probable surface concentration is ∼42 $Å^2$/molecule for SDS and C16TAB and ∼170 $Å^2$/molecule for surfactin. We then used this most probable concentration of each surfactant to simulate NBF with various film thicknesses. From analyzing the disjoining pressure−film thickness isotherms with the density profiles and the solvation coordination number, we found that the increase of the disjoining pressure during the film thinning was coupled with the change in inner structure of the NBF (i.e., density profile and the solvation of ionic entities). In the range of film thicknesses less than ∼30 Å, the disjoining pressures for the SDS and C16TAB were found to be larger than that of the surfactin. We predicted the Gibbs elasticity (175 dyn/cm for surfactin; 109 dyn/cm for C16TAB; 38 dyn/cm for SDS) required to assess the stability of NBF against surface concentration fluctuations, and the shear modulus (6.5 GPa for the surfactin; 6.1 GPa for the C16TAB; 3.5 GPa for the SDS) and the yield stress (∼0.8 GPa for surfactin; ∼0.8 GPa for C16TAB; ∼0.4 GPa for the SDS) to assess the mechanical stability against the externally imposed mechanical perturbation.

1. Introduction

Foam is a colloidal system consisting of a dispersed gas phase and a continuous liquid phase, which tends to spontaneously separate into two distinct bulk phases. Foams are not thermodynamically stable in an absolute sense, but they can be metastable with a significant lifetime.[1−5] In the early stage of foam formation, the continuous liquid phase drains out of the foam because of the gravitational force, and the film thickness decreases. As the thickness between the two surfaces of a foam film decreases, the disjoining pressure increases, eventually preventing the film from draining more of the continuous liquid phase. During this film thinning process, we observed first the common black film (CBF) with ∼10 nm thickness and subsequently the Newton black film (NBF) with <∼5 nm thickness as further thinning occurred.

A number of investigations[1−5] have been made into foam systems because of important applications of foam in our daily life (i.e., fire-fighting foam, polymeric foam insulation, foam rubbers, and personal care products). Many aspects of foam, particularly the structure and properties of the NBF, need further investigation. A general consensus is that foam stability is dominated by various factors depending on the film thickness. First, in the beginning of forming a micrometer-thick film, the drainage rate of the continuous liquid phase is the determining factor for foam stability, and this drainage rate can be controlled to extend the lifetime of foam by adding surfactant.[6−8] As film thinning proceeds down to a thickness of a few nanometers (where the film is regarded as in a quasi-static state without any apparent drainage), the foam stability depends on such physicochemical factors as surfactant adsorption, film structure, surface charge, and surface elasticity,[1−5] all of which affect the molecular interactions between surfactant molecules within a monolayer, as well as the interaction between the two surfactant monolayers within a thin foam film.

The classical Derjaguin, Landau, Verwey, and Overbeek (DLVO) theory[9,10] has successfully predicted and explained the existence and stability of CBF with ∼10−100 nm thickness in terms of repulsive electrostatic interactions and attractive van der Waals interactions between the two surfaces of a foam film. In contrast, the NBF with ∼3−5 nm thickness is not predicted by the classical DLVO theory, because the NBF shows a strong short-range repulsive interaction between the surfaces that cannot be explained in terms of the conventional interactions in the DLVO theory. According to Israelachvili and Wennerstroem,[11] such "nonconventional" interactions are of an entropic nature, arising from the surface structure of the NBF, particularly the density distribution of components. This view seems to be widely accepted as the explanation for the short-range repulsive interaction stabilizing ultrathin NBF.

We should stress, however, that the applicability of such an explanation about the nature of the short-range repulsive interaction depends completely on the knowledge of the structure of NBF. Consequently, it is necessary to determine the details of the structure of NBF. Pioneering attempts have been made to do this using such experimental approaches as thin-film pressure balance,[12] optical measurement,[13] X-ray reflectivity,[14]

* To whom correspondence should be addressed. wag@wag.caltech.edu.

MD Characterization of Newton Black Films

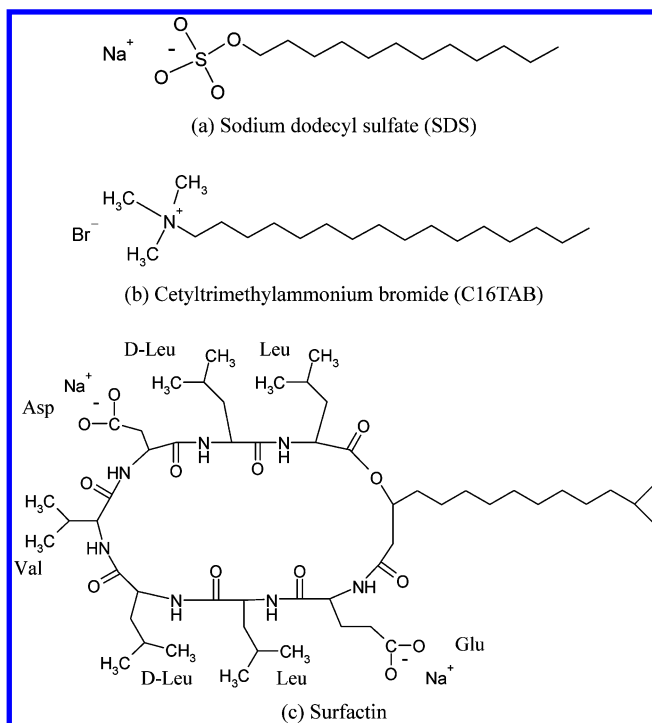*J. Phys. Chem. B, Vol. 110, No. 15, 2006* **7993**

Figure 1. Surfactants used in this study.

FTIR,[15] and gas permeability.[16] Unfortunately, there remain considerable questions about the structure and properties of NBF.

Although in this context we expect molecular modeling approaches such as molecular dynamics (MD) and Monte Carlo (MC) simulations to take an important role to provide atomistic or molecular details of NBF, just a few pioneering MD studies have been reported for foam (thin liquid film) systems:[17−20] Klein and co-workers[17] reported the first MD study on the SDS-mediated NBF in which the simulated film structures are found in a good agreement with the X-ray reflectivity experiments; Weng et al.[18] investigated a Lennard-Jones liquid thin film using MD simulation and discussed that the surface tension distribution is affected by the film thickness. The first disjoining pressure−thickness isotherm was reported by Radke and co-workers for the Lennard-Jones thin film[19] and water thin film,[20] discussing the Lifshitz theory in comparison with their simulations.

In this paper, we also apply molecular dynamics (MD) methods to provide essential information on the structures and properties of various interfacial systems. Here, we use techniques documented in previous studies of the surfactant-mediated decane−water interface,[21] the amphiphilic molecular self-assembled monolayer on Au (111),[22] and the Langmuir monolayer at air−water interface.[23]

In this study, we performed atomistic molecular dynamics (MD) simulations to obtain detailed information on the structures and properties of NBFs for such surfactants as the following:

• sodium dodecyl sulfate (SDS, Figure 1a), a chemical surfactant;

• cetyltrimethylammonium bromide (C16TAB, Figure 1b), a chemical surfactant;

• surfactin (Figure 1c), a biosurfactant produced by various strains of *Bacillus subtilis*.[24]

SDS and C16TAB are widely used surfactants for both academic research and industrial production. Despite its excellent interfacial activity[25−27] and diverse bioactivities,[25,26,28−31]

the NBF of surfactin has not previously been studied, so almost nothing has been reported in terms of its structure and properties.

To simulate the NBF of these surfactants, we first predicted the surface pressure−area isotherm for various surface concentrations to determine the most probable surface concentration in the presence of the water phase. Then, using this most probable surface concentration (assuming it to be constant over the range of NBF thickness), we predicted the NBFs as a function of film thickness. In this study, we compare the structures and properties of the NBF made of each surfactant and discuss the stability of these NBFs.

2. Simulation Details

2.1. Force Field and MD Parameters. We employed the Dreiding force field,[32] a generic force field suitable for all main group organic systems. In addition, we used the F3C model[33] to describe water and the united atom model[34−37] to describe the alkyl tail part of the surfactant. However, the hydrophilic polar head of the surfactant was described with a full explicit atom model. This force field is the same as we used in previous studies of the surfactant-mediated decane−water interface.[21]

The total potential energy is given in eq 1

$$E_{total} = E_{vdW} + E_Q + E_{bond} + E_{angle} + E_{torsion} + E_{inversion} \quad (1)$$

where E_{vdW}, E_Q, E_{bond}, E_{angle}, $E_{torsion}$, and $E_{inversion}$ are the van der Waals, electrostatic, bond-stretching, angle-bending, torsion, and inversion components, respectively. For the vdW interactions between different atomic species, we used the standard geometric mean combination rules. The detailed force field parameters have been reported previously.[21]

The atomic charges of surfactant were assigned using the charge equilibration (QEq) method,[38] as in our previous study.[21] The atomic charges of the water molecules were taken from the F3C water model.[33] To accurately describe the long-range electrostatic interactions, we used the particle−particle, particle-mesh Ewald (PPPM) method.[39]

To control the temperature, we used a Nose−Hoover thermostat[40,41] with a relaxation time of 0.1 ps. The equations of motion were integrated using the velocity−Verlet algorithm[42] with a time step of 1.0 fs. The MD software employed in this study was the LAMMPS (large-scale atomic/molecular massively parallel simulator)[43,44] code from Sandia National Laboratories, modified to run our Dreiding force field.

2.2. Model and MD Simulation. To simulate the NBF of each surfactant, we constructed the system as follows. First, we packed 16 molecules for SDS and C16TAB to form a surfactant monolayer with spacing suitable for hexagonal close packing but in an orthorhombic simulation box with periodic boundary conditions applied for all three spatial directions as shown in Figure 2a. For surfactin, we used the same procedure except with 4 molecules per periodic cell. Thus, the total number of independent surfactant molecules in the system was 32 for SDS and C16TAB and 8 for surfactin. The smaller number for surfactin was used, because the molecular area of surfactin is about 4 times larger than that of SDS and C16TAB. After preparing the surfactant monolayer for each surfactant, we put them on top of a slab of water (Figure 2b) and equilibrated the system using MD.

To determine the most probable surface concentration, we prepared monolayers with coverage ranging from 21.65 to 86.60 Å² per molecule for SDS and C16TAB and from 124.71 to 221.70 Å² per molecule for the surfactin. This was done by setting the value of unit cell parameters $a = b$ (Figure 2a) to
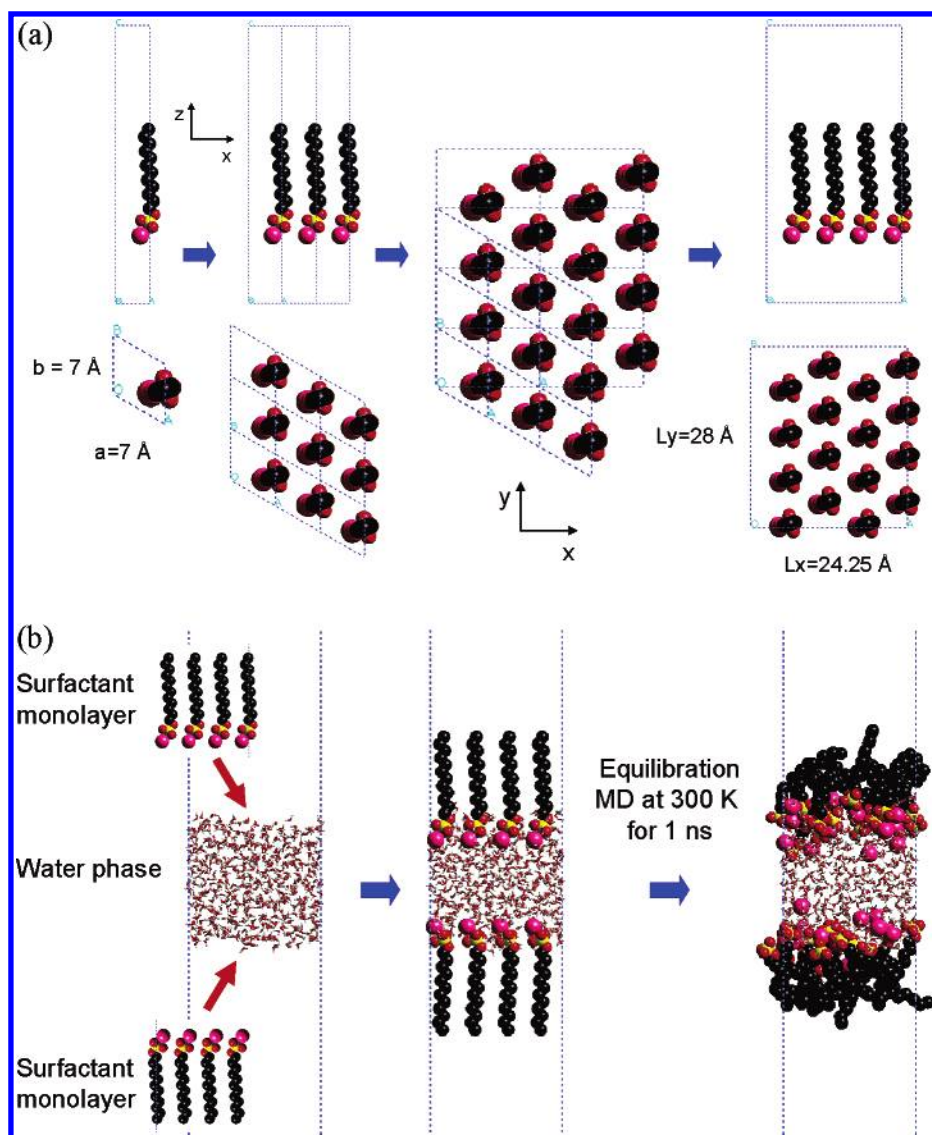
Figure 2. (a) Preparation of initial configuration of surfactant monolayer: A hexagonal closed-packing mode was retained in an orthorhombic simulation box consisting of 16 molecules for SDS and C16TAB and 4 molecules for surfactin at one surface. (b) Two SDS surfactant monolayers (packing of 42.44 Å²/molecule) were integrated with a water phase to make Newton Black film.

TABLE 1: Composition and Dimensions of Simulated System

			SDS & C16TAB			
			No. of Surfactant/System = 32			
system	$a = b$ (Å)	L_x (Å)	L_y (Å)	L_z (Å)	no. of water molecules	area/molecule (Å²)
5×5	5	17.32	20.00	300	320	21.65
6×6	6	20.78	24.00		440	31.18
7×7	7	24.25	28.00		545	42.44
8×8	8	27.71	32.00		808	55.43
10×10	10	34.64	40.00		1210	86.60
			Surfactin			
			No. of Surfactant/System = 8			
system	$a = b$ (Å)	L_x (Å)	L_y (Å)	L_z (Å)	no. of water molecules	area/molecule (Å²)
12×12	12	20.78	24.00	300	440	124.71
13×13	13	22.52	26.00		468	146.36
14×14	14	24.25	28.00		545	169.74
15×15	15	25.98	30.00		619	194.86
16×16	16	27.71	32.00		808	221.70

the values summarized in Table 1. Then, we minimized the energy to relax the surfactant monolayer within the dimensions of the fixed simulation box. Next, we placed this surfactant monolayer on both sides of water with the same cell parameters and energy-minimized to obtain the optimum interaction between the surfactant monolayer and the water subphase.

Then, starting with the above initial configuration, we carried out NVT MD simulations at 300 K for 1 ns to equilibrate the system (Figure 2b). Then, starting with this equilibrated system, we continued the MD for another 4 ns to evaluate the properties. This was done for each fixed surface area per molecule to find the most probable surface concentration for each surfactant (see section 3.1 for further discussion). Figure 3a shows snapshots of equilibrated films for various surface concentrations (packings) with the same thickness (∼20 Å) of the water phase.

Assuming that the most probable surface concentration for each surfactant is retained during the film thinning, we obtain the NBF for various film thicknesses of each surfactant. Figure 3b shows the NBFs with various film thicknesses after 4 ns NVT MD equilibration for each thickness. This simulation of NBF leads to the thickness-dependent properties such as disjoining pressure−thickness isotherm.

3. Results and Discussion

3.1. Surface Pressure−Area Isotherm and Most Probable Surface Concentration. The predicted surface pressure−area

MD Characterization of Newton Black Films

J. Phys. Chem. B, Vol. 110, No. 15, 2006 **7995**
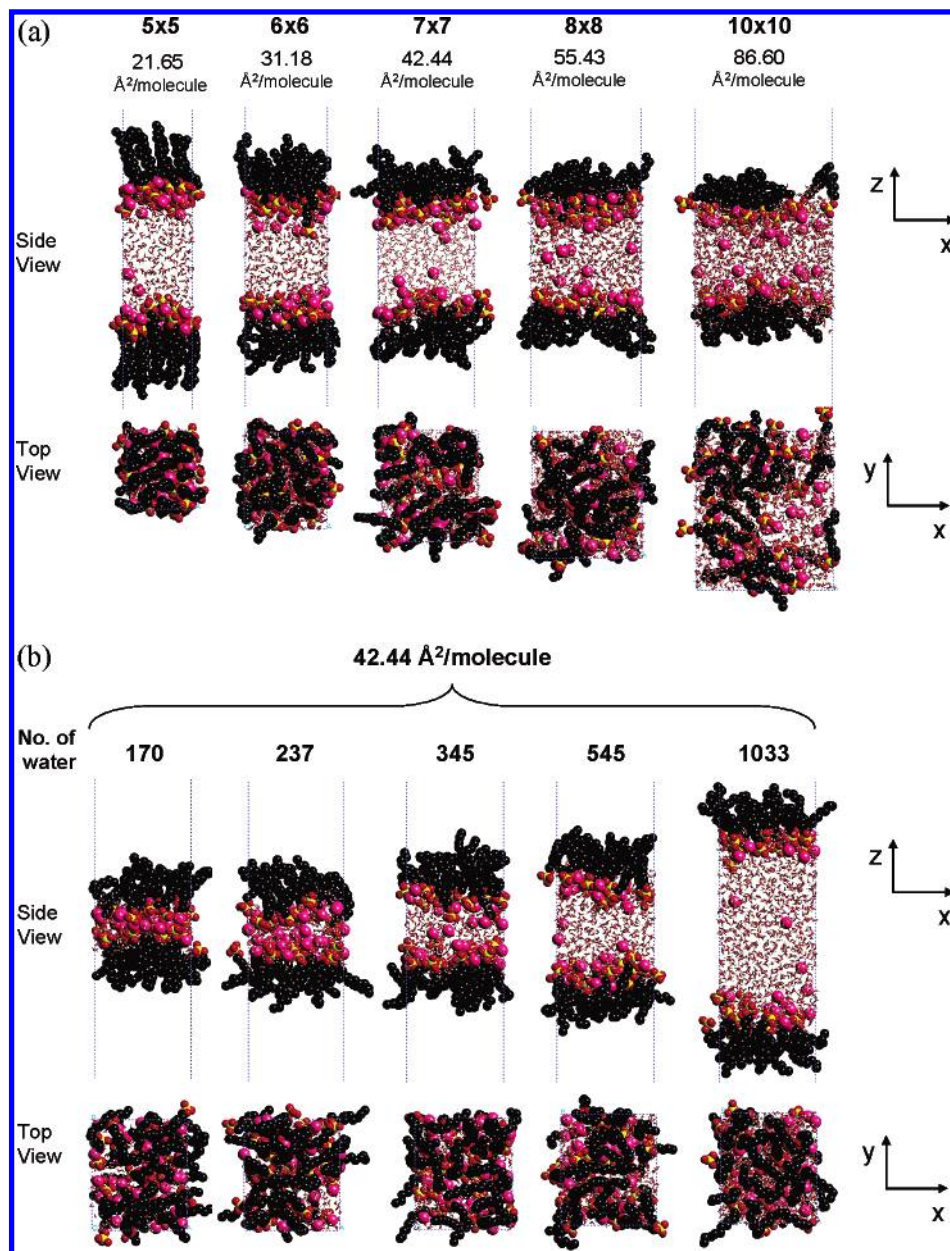
Figure 3. Snapshots of the equilibrated systems: (a) with various surface concentrations and the same water phase thickness ($\sim$20 Å) as summarized in Table 1; (b) with various NBF thickness and the same surface concentration (42.44 Å²/molecule). Presented is the case of SDS.

isotherms for each surfactant are reported in Figure 4a. The experimental surface pressure–area isotherm is obtained using a Langmuir trough, where the surface pressure (or surface tension) to compress the movable barrier to various areas is measured. The definition of surface pressure ($\Pi_{\text{surface}}(A)$) is

$$\Pi_{\text{surface}}(A) = \sigma_0 - \sigma \qquad (2)$$

where A is the area per molecule, σ_0 is the surface tension of the air–water interface, and σ is the value for the air–surfactant–water interfacial system (Langmuir monolayer). To calculate σ_0 and σ, using the following definition

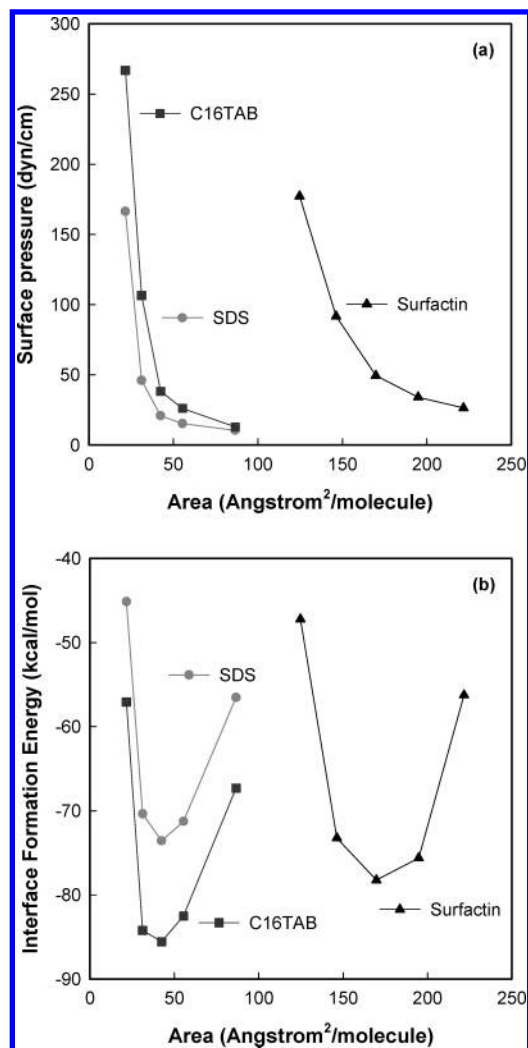$$\sigma = \frac{1}{2} \int_0^L dz [P_N(z) - P_T(z)] \qquad (3)$$

we sliced the system into slabs with 1.5 Å thickness parallel to the *xy* (water) plane and calculated the normal and tangential components of the stress ($P_N(z)$ and $P_T(z)$) of each slab using the Kirkwood–Buff theory[45] as we have done

in our previous studies[21–23]

$$P_N(z) = \rho(z)k_B T - \frac{1}{V_{\text{slab}}} \left\langle \sum_{i,j} \frac{z_{ij}^2}{r_{ij}} \frac{du(r_{ij})}{dr_{ij}} \right\rangle \qquad (4)$$

$$P_T(z) = \rho(z)k_B T - \frac{1}{V_{\text{slab}}} \left\langle \sum_{i,j} \frac{x_{ij}^2 + y_{ij}^2}{2r_{ij}} \frac{du(r_{ij})}{dr_{ij}} \right\rangle \qquad (5)$$

where L is the dimension of the system in the *z*-axis direction, and $\rho(z)$ and V_{slab} denote the density of the slab at z and the slab volume, respectively, and k_B and T are the Boltzmann constant and the absolute temperature, respectively. Angle brackets mean an ensemble average of all atoms located in the slab at z. r_{ij}, x_{ij}, y_{ij}, and z_{ij} are the distances between the atoms and their coordinate components, respectively, and $u(r_{ij})$ is the potential energy of the atomic pair i and j. Using this method with MD simulations in our previous study,[21] we could obtain the surface tension (interfacial tension) values for the interfacial

7996 *J. Phys. Chem. B, Vol. 110, No. 15, 2006*

Jang and Goddard

Figure 4. (a) Change in surface pressure as a function of surface concentration. (b) Change in interface formation energy as a function of surface concentration.

TABLE 2: Most Probable Surface Concentration and Surface Tension at that concentration

	most probable surface concentration (Å²/molecule)		surface tension (dyn/cm)	
T = 300 K	simulation	experiment	simulation	experiment
water			70.94	71.71[a]
SDS	42.44	33−52[b]	44.02	38.4[c]
C16TAB	42.44	42−44[d,e]	32.66	38[e]
surfactin	169.74	NA	22.23	NA

[a] Refs 47,48. [b] Refs 14, 70−73. [c] Ref 74. [d] Ref 75. [e] Ref 76.

• $E_{air-water}$ denotes the bare air−water system obtained from a separate 800 ps MD simulation of a water slab with the same number of water molecules used in the total system at the same temperature.
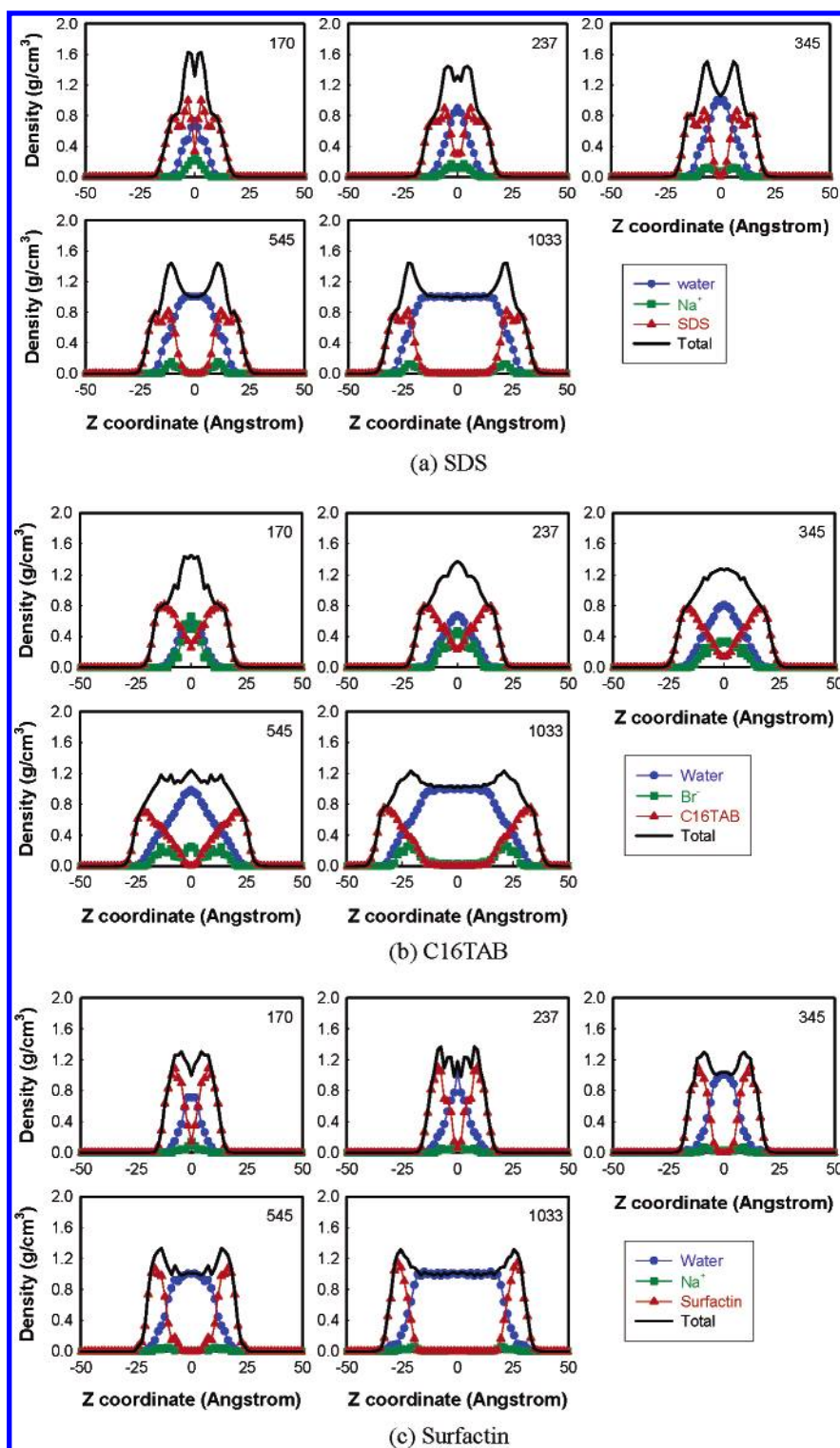
The IFE value is a measure of the average intermolecular interaction per surfactant molecule arising from insertion of one surfactant molecule into the air−water interface. Figure 4b shows the change of IFE as a function of surface concentration. All surfactants used in this study led to the same behavior (showing a minimum at the surface concentration corresponding to the most stable state energetically). The predicted most probable surface concentration and the corresponding surface tension for each surfactant (Table 2) show a good agreement with experiment.

3.2. Effect of NBF Thickness. Using the most probable surface concentration discussed in the previous section, we predicted the NBF of each surfactant for various film thicknesses. As mentioned above, we assumed that this most probable surface concentration was retained for various film thicknesses. This is plausible since film drainage-driven thinning is essentially stopped in this quasi-static state.

3.2.1. Density Profile and Inner Structure of NBF. Figure 5 shows the density profiles of each system along the *z*-axis direction of the simulation box. This was obtained by partitioning the system into 1.5-Å-thick slabs parallel to the *xy*-plane. The total density profile is decomposed into the contributions from the main components: water, surfactant, and counterions to provide the distribution of each component throughout the NBF.

These density profiles and the snapshots of the equilibrated structures of NBF (Figure 3) show clearly that the NBF has a well-organized self-assembled feature: Two surfactant monolayers cover the water phase, and the hydrophilic head parts are solvated into the water phase. To quantify the change of thickness as a function of the number of water molecules, we define the "90−90 thickness" as the distance between two points where the density of the surfactant monolayer is 90% of its maximum value (Figure 6). Since the number of surfactant molecules and the surface area per molecule were invariant throughout the simulations for the various thicknesses, the NBF thickness increased linearly as the number of water molecule increased.

These density profiles show that, when the film thickness becomes less than ∼30 Å (the number of water molecules per ionic group is 10−20), the two surfactant monolayers start contacting each other. For these ultrathin contacting dimensions, we find that the inner structures of the NBF, particularly, the solvation of the ionic head part of surfactant by water, are affected. The counterions (Na⁺ for SDS and surfactin; Br⁻ for C16TAB) stay with the hydrophilic ionic head parts inside the water phase. Such binding of counterions to the ionic surfactant at the interface has been well-characterized with both experiment[50] and theory[51] over a wide range of surfactant concentra-

systems such as air−decane (21.77 ± 2.31 dyn/cm; exptl[46] 23.20 dyn/cm), air−water (70.94 ± 2.25 dyn/cm; exptl[47,48] 71.71 dyn/cm), and decane−water (54.70 ± 3.62 dyn/cm; exptl[49] 51.72 dyn/cm). The surface pressure−area isotherms are presented in Figure 4a. First, it is clearly observed (Figure 4a) that the surface pressure (Π) decreases with increasing area/molecule, so that the value of Π approaches zero (the surface pressure of bare water surface) as the surface concentration becomes dilute. This behavior is a common one for the surface pressure experimentally observed in general amphiphilic molecules.

Since this surface pressure−area isotherm provide the information about the relationship between the surface pressure (and surface tension) and the molecular packing at the air/water interface, but not the information about which surface concentration is preferred for each surfactant as "the most probable surface concentration", to find the most probable surface concentration, we evaluated the interface formation energy (IFE)[21] defined as follows:

$$IFE = \frac{E_{total} - (n \times E_{surfactant,single} + E_{air-water})}{n} \quad (6)$$

where
• E_{total} denotes the energy of the whole system;
• $E_{surfactant,single}$ denotes the single surfactant molecule calculated from a separate 100 ps MD simulation in a vacuum at the same temperature;

MD Characterization of Newton Black Films

J. Phys. Chem. B, Vol. 110, No. 15, 2006 **7997**

Figure 5. Density profiles of NBFs with various thicknesses for each surfactant. Number in each plot denotes the number of water molecules.

tions, especially above the critical micelle concentration (cmc) in the absence of additional background salt concentration; thus, the distribution of counterions we find in our simulations is in good agreement with previous studies.

To investigate the inner structures of NBF, we calculated the coordination number from the pairwise radial distribution function (RDF) of the following

- the oxygen (water)−oxygen (water) pair;
- the counterion (Na^+ for SDS and surfactin; Br^- for C16TAB)−oxygen (water) pair;

- the polar head (sulfur for SDS; nitrogen for C16TAB; carboxylic carbon for surfactin)−counterion pair

by integrating the first solvation shell. Figure 7a shows that the water coordination number increases rapidly toward the value for the bulk water (4.6 in our simulation[21] and 4.5 in experiment[52]) with increasing film thickness. The water structure near the interface deviates from that of the bulk phase due to the solvation of the hydrophilic ionic head part of surfactants and their counterions in addition to the existence of the interface itself.

7998 *J. Phys. Chem. B, Vol. 110, No. 15, 2006*

Jang and Goddard
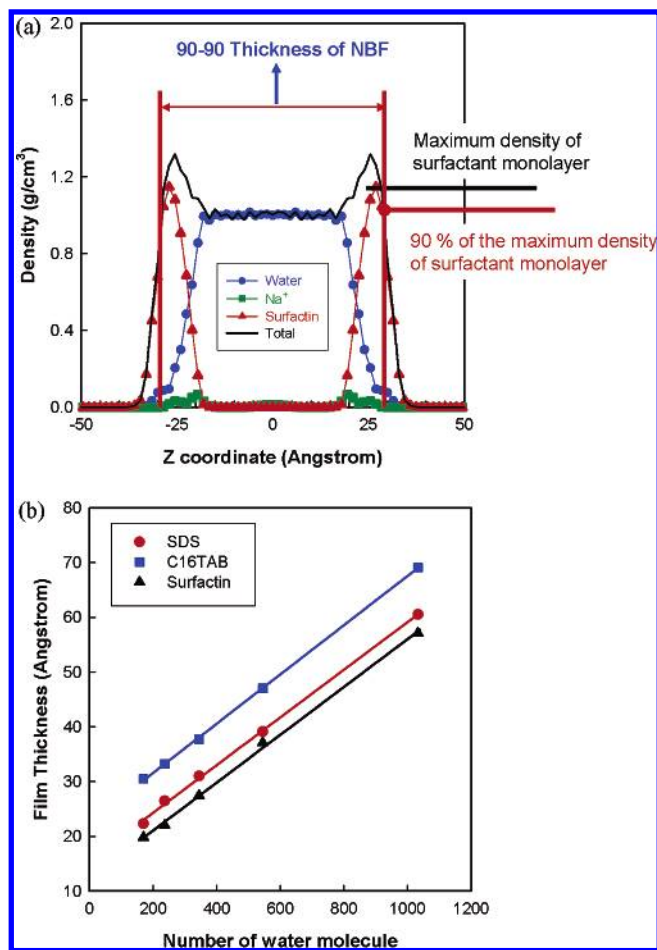
Figure 6. (a) The "90−90 thickness" of NBF is the distance between the two points where the density of the surfactant monolayer is 90% of its maximum value. Presented is the case of surfactin with 1033 water molecules. (b) Change of film thickness as a function of the number of water molecule. The solid lines are from the least-squares fit.

The solvation of the counterion by water is shown in Figure 7b. With increasing film thickness, the water coordination number for the counterions increases toward the value in bulk water, which is $5.4−6.0^{53−56}$ for Na^+ and 6.9^{57} for Br^-. An interesting feature in Figure 7b is that the water coordination number of Na^+ for surfactin is not reduced as much as that for SDS, which raises a question of how the Na^+ ion of surfactin can retain its water neighbors in comparison with the Na^+ ion of SDS. The concentration of Na^+ in surfactin NBF is half of that in SDS NBF, which we suspect helps the Na^+ ion remain solvated in NBF even when the thickness is less than ∼40 Å.

Next, we analyzed the relationship of the ionic group (sulfate of SDS, trimethylammonium of C16TAB, and carboxylate of surfactin) with its counterion by counting the number of counterions surrounding the ionic group in the first solvation shell. As shown in Figure 7c, for all cases, the counterion coordination number decreases with increasing film thickness. However, it is obvious that such a decrease of coordination number for the surfactin is much less than that for SDS and C16TAB. This is explained as follows. For a thin NBF with thickness less than ∼40 Å, the two surfactant monolayers contact each other (consistent with the density profiles of Figure 5). Thus, for an NBF with a relatively high surfactant concentration (high ionic head concentration) such as SDS and C16TAB, the contribution of counterions can be attributed to both monolayers, while for an NBF with a low surfactant concentration such as
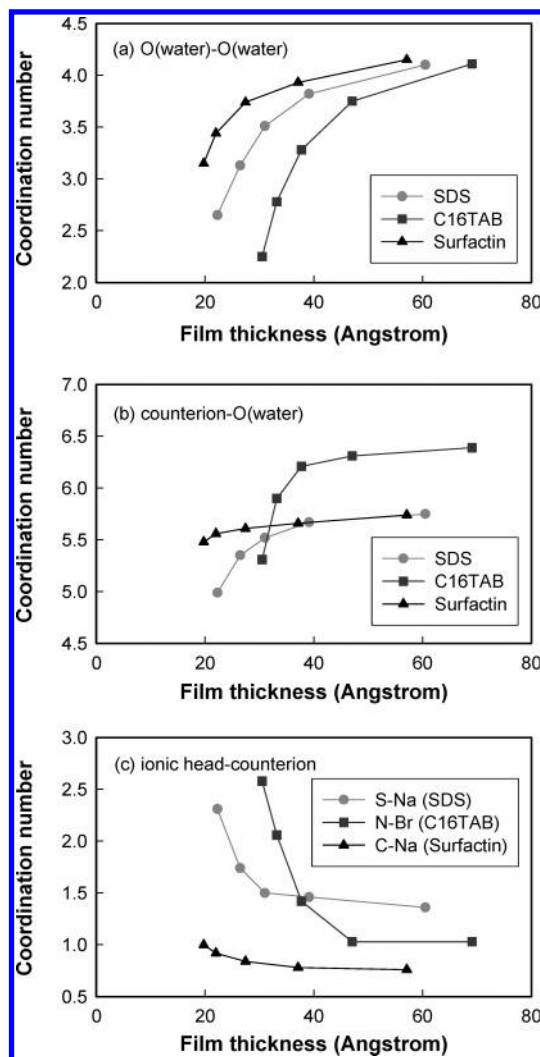

Figure 7. (a) Change of water−water coordination number. (b) Change of counterion−water coordination number. (c) Change of ionic head−counterion coordination number as a function of film thickness.

surfactin, the counterion contributes to just one of either of the monolayers.

3.2.2. Disjoining Pressure−Film Thickness Isotherm. We calculated the disjoining pressure−film thickness isotherms from the simulations in order to understand how the atomistic structural details affect this stability of the NBF. The disjoining pressure, $\Pi_{disjoin}(h)$ is equal to the difference between the surface normal component of pressure in the film (P_N) and the pressure in the homogeneous liquid (P_L)[58]

$$\Pi_{disjoin}(h) = P_N - P_L \qquad (7)$$

where h is the film thickness. According to this definition, the disjoining pressure is a function of thickness; when the external pressure changes, the film thickness responds by changing until a new balance is achieved between the external pressure and the disjoining pressure. When the applied external pressure is larger than the maximum disjoining pressure, the foam film ruptures. Thus, this disjoining pressure is a measure of the film stability in the quasi-static-state regime, where the drainage does not proceed effectively. It will be interesting to compare the forces characterizing the CBF from those that stabilize the NBF, since the latter is not well-described in classical DLVO theory.

MD Characterization of Newton Black Films

J. Phys. Chem. B, Vol. 110, No. 15, 2006 **7999**
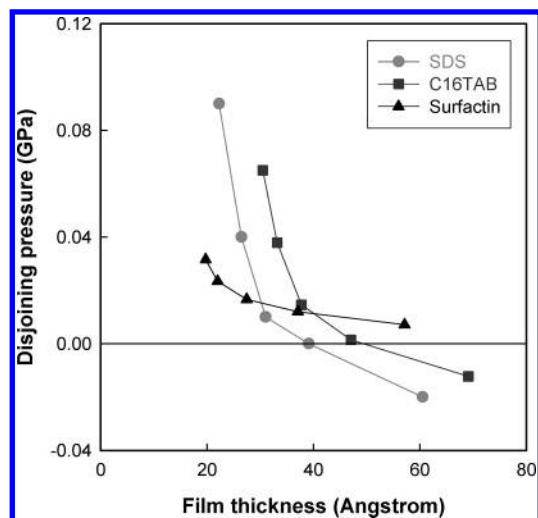
Figure 8. Disjoining pressure−film thickness isotherm for each surfactant.

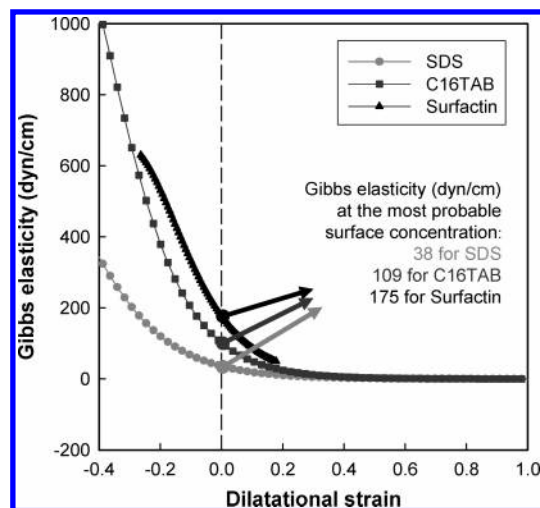**Figure 9.** Change of Gibbs elasticity as a function of dilatational strain.

Figure 8 shows the disjoining pressure isotherm for each surfactant (the thickness of stable NBF is at 1 atm). This shows that the thickness of stable NBF is ∼40 Å for SDS, which agrees with the experimental value (33−44 Å),[13,14] supporting the validity of our simulations. For the C16TAB, we predict ∼47 Å for the stable NBF thickness, but we could not find experimental data to compare with this. For the surfactin case, we do not find the stable NBF thickness in the range of thicknesses simulated in this study, but extrapolating the trend in the disjoining pressure−thickness isotherm of surfactin suggests that the thickness of a stable NBF is beyond 100 Å.

The range of thickness for which the disjoining pressure has positive slope is regarded as being unstable, because in that regime, the film thinning should proceed spontaneously until film rupture occurs.[3] With this criterion, all NBFs over the whole range of film thickness simulated in this study would be stable. However, the disjoining pressure of SDS and C16TAB increase with decreasing film thickness more rapidly than surfactin. Why is surfactin different from SDS and C16TAB? One possibility is the structural dissimilarity of surfactin from SDS and C16TAB. First, Figure 5a,b shows clearly that the two surfactant monolayers in the NBF for SDS and C16TAB have merged into each other when the thickness is less than ∼40 Å, whereas Figure 5c for surfactin shows that the merger has barely occurred even for the thinnest NBF.

In addition, we found a similar difference in the counterion distribution. In contrast to SDS and C16TAB, the counterions in the surfactin NBF show a much lower tendency to merge into one layer. These features are coupled with the solvation of counterion and ionic head part: Figure 7b shows that the solvation of ionic entities for SDS and C16TAB degrades as film thinning proceeds, whereas the dissociation of surfactin was little influenced by the film thinning. If the state of the ionic form in the bulk water phase is considered as a reference, the changes in ionic solvation caused by film thinning drives the NBF toward a more unfavorable state. Consequently, on the basis of these disjoining pressure−film thickness isotherms, we consider that the NBF of SDS and C16TAB have more stability against the film thinning than that of the surfactin.

3.3. Gibbs Elasticity and Mechanical Shear Deformation. In addition to the film stability against film thinning, we examined the film stability against the transverse perturbations. For this purpose, we calculated the Gibbs elasticity (E)

defined as

$$E = \frac{d\sigma}{d \ln A} \tag{8}$$

where σ denotes the surface tension and A is the surface area. Physically, the Gibbs elasticity indicates the capacity of the film to increase its tension upon the surface dilatation of the film. This can also be interpreted as a stability to resist surface concentration fluctuations by retaining a uniform surfactant packing at a given pressure and temperature. Thus, Gibbs elasticity is related to the stability provided by intermolecular interactions between the surfactant molecules, while the disjoining pressure relates to the structure reorganization occurring in the water and solvation of hydrophilic ionic entities. For this reason, the Gibbs elasticity has been studied extensively.[59−66] Figure 9 shows the change of the Gibbs elasticity calculated using the data shown in Figure 4a as a function of the dilatational strain

$$\text{Dilatational strain} = \frac{(A - A_0)}{A_0} \tag{9}$$

where A is the area occupied by each surfactant and A_0 is the reference area corresponding to the most probable surface concentration. Our results indicate that a common feature of the three surfactants is that the Gibbs elasticity decays with increasing the dilatational strain. This means that the foam film cannot store the two-dimensional elastic energy in order to recover to the original packing as the surfactant monolayer loses its molecular self-assembled nature. As shown in Figure 9, we predict that the Gibbs elasticity at the most probable concentration is 175 dyn/cm for surfactin, 109 dyn/cm for C16TAB, and 38 dyn/cm for surfactin. This indicates that surfactin NBF would form a monolayer on the water more stable against the surface concentration fluctuation.

We are also interested in is the mechanical response to a shear deformation externally imposed on the NBF. We find that shear deformation simulations provide information on how large a stress the NBF can endure before it undergoes permanent deformation at a fixed concentration. In reality, this shear deformation may be accompanied by the concentration fluctuations, but here, we analyzed only the contribution of mechanical stability of NBF by factoring out the contribution of Gibbs elasticity.
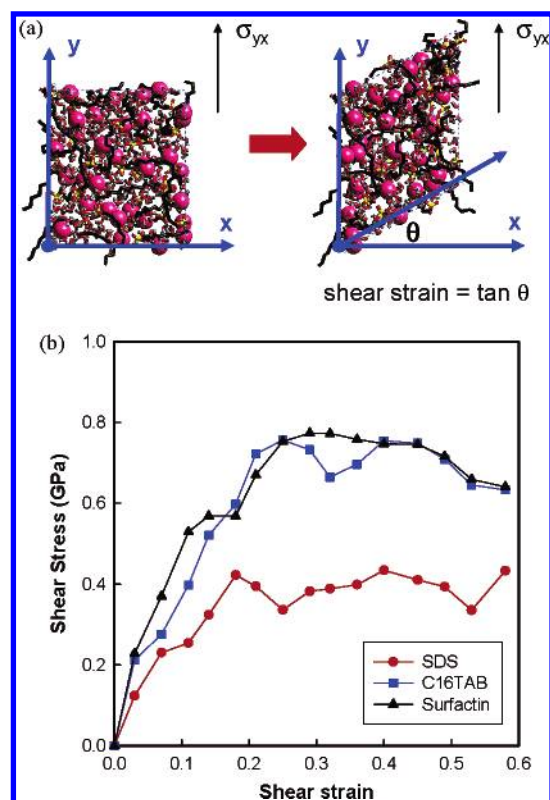
Figure 10. (a) Simple shear deformation of NBF. The extent of deformation is measured by the shear strain defined as tan θ. The pictures are from the top view of the NBF of SDS. The surface concentration is constant before and after this deformation. (b) Shear stress−shear strain curves obtained from these simple shear deformations.

For this purpose, we imposed a quasi-static mechanical deformation[67−69] of the NBF from which we calculated the change of shear stress component (σ_{yx}) as a function of shear strain (tan θ) using the energy minimization as shown in Figure 10a. Each shear stress−shear strain curve in Figure 10b is the average from the five NBFs of each surfactant with various thicknesses. It is clear that the NBF of each surfactant has a common mechanical response: All curves consist of an elastic regime at small strain (up to ∼0.1) and a plastic regime at large strain. The shear elastic modulus was calculated as 3.5 GPa for SDS, 6.1 GPa for C16TAB, and 6.5 GPa for surfactin, indicating that the NBF for surfactin and C16TAB store more elastic deformation energy than the SDS NBF, thereby leading to a better recovery from the deformed state. Another noteworthy point is that the yield stress is the maximum stress the NBF can endure. In other words, if the NBF is under a stress beyond the yield stress, its structure easily undergoes an irrecoverable deformation until it ruptures. We found from Figure 10b that the yield stress was ∼0.8 GPa for both C16TAB and surfactin, and ∼0.4 GPa for SDS, indicating that the NBFs of C16TAB and surfactin are tougher than that of SDS.

4. Summary

We used MD simulations to determine the structures and properties of NBFs formed from surfactants SDS, C16TAB, and surfactin. We determined the most probable surface concentration for each surfactant monolayer on the water phase, and we obtained the surface pressure−area isotherm and the interface formation energy (IFE) at each surface concentration. We found that the most probable surface concentration is 42 Å²/molecule

for SDS and C16TAB and 170 Å²/molecule for surfactin, which yields the lowest value of IFE.

Using these concentrations, we simulated the NBF for various film thicknesses up to 10 nm. We analyzed the density profiles to find a well-organized self-assembled feature of NBF in which the hydrophilic parts are well-associated with the water phase, but eventually merge into one as the film thickness decreases below 30 Å for SDS and surfactin and below 40 Å for C16TAB. In addition, we analyzed the coordination number of the water and the ionic entities in the NBF, showing that, as the film thickness decreases, the water structure and the solvation of counterion (Na$^+$ for SDS and surfactin; Br$^-$ for C16TAB) deviates significantly from that in bulk water.

We calculated the disjoining pressure−film thickness isotherms and found a common feature that the disjoining pressure increases with decreasing film thickness. We also found that the change of disjoining pressure is strongly coupled to the change in the inner structure of the NBF, such as the density profile and the solvation of ionic entities. A large increase in disjoining pressure seems to be induced by the rapid change in the inner structure for thin films. We found that, for the NBF with the film thickness less than ∼30 Å, SDS and C16TAB showed a larger disjoining pressure than surfactin.

The calculated Gibbs elasticity (175 dyn/cm for surfactin; 109 dyn/cm for C16TAB; 38 dyn/cm for SDS) indicates that surfactin has a better stability against the surface concentration fluctuations than either C16TAB or SDS. In addition, the mechanical shear modulus (6.5 GPa for surfactin; 6.1 GPa for C16TAB; 3.5 GPa for SDS) and yield stress (∼0.8 GPa for surfactin and C16TAB; ∼0.4 GPa for SDS) indicate that surfactin and C16TAB are mechanically more stable than SDS.

References and Notes

(1) Myers, D. *Surfactant Science and Technology*; VCH: New York, 1946.
(2) Pugh, R. J. *Adv. Colloid Interface Sci.* **1996**, *64*, 67−142.
(3) Bhakta, A.; Ruckenstein, E. *Adv. Colloid Interface Sci.* **1997**, *70*, 1−124.
(4) Bergeron, V. *J. Phys.: Condens. Matter* **1999**, *11*, R215−R238.
(5) Stubenrauch, C.; Klitzing, R. v. *J. Phys.: Condens. Matter* **2003**, *15*, R1197−R1232.
(6) Danov, K. D.; Valkovska, D. S.; Ivanov, I. B. *J. Colloid Interface Sci.* **1999**, *211*, 291−303.
(7) Valkovska, D. S.; Danov, K. D.; Ivanov, I. B. *Colloids Surf., A* **2000**, *175*, 179−192.
(8) Valkovska, D. S.; Danov, K. D.; Ivanov, I. B. *Adv. Colloid Interface Sci.* **2002**, *96*, 101−129.
(9) Derjaguin, B. V. *Theory of Stability of Colloids and Thin Films*; Consultants Bureau: New York, 1989.
(10) Verwey, E. J. W.; Overbeek, J. T. G. *Theory of the Stability of Lyphobic Colloids, the Interaction of Sol Particles Having and Electric Double Layer*; Elsevier: New York, 1948.
(11) Israelachvili, J. N.; Wennerstroem, A. *J. Phys. Chem.* **1992**, *96*, 520−531.
(12) Claesson, P. M.; Ederth, T.; Bergeron, V.; Rutland, M. W. *Adv. Colloid Interface Sci.* **1996**, *67*, 119−183.
(13) Jones, M. N.; Mysels, K. J.; Scholten, P. C. *Trans. Faraday Soc.* **1966**, *62*, 1336−1348.
(14) Belorgey, O.; Benattar, J. J. *Phys. Rev. Lett.* **1991**, *66*, 313−316.
(15) Tian, Y. C. *J. Phys. Chem.* **1991**, *95*, 9985−9988.

MD Characterization of Newton Black Films

J. Phys. Chem. B, Vol. 110, No. 15, 2006 **8001**

(16) Krustev, R.; Platikanov, D.; Nedyalkov, M. *Colloids Surf., A* **1993**, *79*, 129−136.

(17) Gamba, Z.; Hautman, J.; Shelly, J. C.; Klein, M. L. *Langmuir* **1992**, *8*, 3155−3160.

(18) Weng, J.-G.; Park, S.; Lukes, J. R.; Tien, C.-L. *J. Chem. Phys.* **2000**, *113*, 5917−5923.

(19) Bhatt, D.; Newman, J.; Radke, C. J. *J. Phys. Chem. B* **2002**, *106*, 6529−6537.

(20) Bhatt, D.; Newman, J.; Radke, C. J. *J. Phys. Chem. B* **2003**, *107*, 13076−13083.

(21) Jang, S. S.; Lin, S. T.; Maiti, P. K.; Blanco, M.; Goddard, W. A.; Shuler, P.; Tang, Y. C. *J. Phys. Chem. B* **2004**, *108*, 12130−12140.

(22) Jang, S. S.; Jang, Y. H.; Kim, Y. H.; Goddard, W. A.; Flood, A. H.; Laursen, B. W.; Tseng, H. R.; Stoddart, J. F.; Jeppesen, J. O.; Choi, J. W.; Steuerman, D. W.; Delonno, E.; Heath, J. R. *J. Am. Chem. Soc.* **2005**, *127*, 1563−1575.

(23) Jang, S. S.; Jang, Y. H.; Kim, Y.-H.; Goddard, W. A., III; Choi, J. W.; Heath, J. R.; Laursen, B. W.; Flood, A. H.; Stoddart, J. F.; Norgaard, K.; Bjornholm, T. *J. Am. Chem. Soc.* **2005**, *127*, 14804−14816.

(24) Ullrich, C.; Kluge, B.; Palacz, Z.; Vater, J. *Biochemistry* **1991**, *30*, 6503−6508.

(25) Arima, K.; Kakinuma, A.; Tamura, G. *Biochem. Biophys. Res. Commun.* **1968**, *31*, 488−494.

(26) Kakinuma, A.; Tamura, G.; Arima, K. *Separatum Exp.* **1968**, *24*, 1120−1121.

(27) Marget-Dana, R.; Ptak, M. *J. Colloid Interface Sci.* **1992**, *153*, 285−291.

(28) Kameda, Y.; Matsui, K.; Kato, H.; Yamada, T.; Sagai, H. *Chem. Pharm. Bull.* **1972**, *20*, 1551−1557.

(29) Kameda, Y.; Ouhira, S.; Matsui, K.; Kanatomo, S.; Hase, T.; Atsusaka, T. *Chem. Pharm. Bull.* **1974**, *20*, 938−944.

(30) Hosono, K.; Suzuki, H. *J. Antibiot.* **1983**, *36*, 667−673.

(31) Hosono, K.; Suzuki, H. *J. Antibiot.* **1983**, *36*, 679−683.

(32) Mayo, S. L.; Olafson, B. D.; Goddard, W. A., III *J. Phys. Chem.* **1990**, *94*, 8897−8909.

(33) Levitt, M.; Hirshberg, M.; Sharon, R.; Laidig, K. E.; Daggett, V. *J. Phys. Chem. B* **1997**, *101*, 5051−5061.

(34) Siepmann, J. I.; Karaborni, S.; Smit, B. *Nature (London)* **1993**, *365*, 330−332.

(35) Smit, B. *Phys. Rev. A* **1988**, *37*, 3431−3433.

(36) Smit, B.; Hilbers, P. A. J.; Esselink, K.; Rupert, L. A. M.; Vanos, N. M.; Schlijper, A. G. *J. Phys. Chem.* **1991**, *95*, 6361−6368.

(37) Smit, B.; Karaborni, S.; Siepmann, J. I. *J. Chem. Phys.* **1995**, *102*, 2126−2140.

(38) Rappe, A. K.; Goddard, W. A. *J. Phys. Chem.* **1991**, *95*, 3358−3363.

(39) Hockney, R. W.; Eastwood, J. W. *Computer Simulation Using Particles*; McGraw-Hill International Book Co.: New York, 1981.

(40) Nose, S. *J. Chem. Phys.* **1984**, *81*, 511−519.

(41) Hoover, W. G. *Phys. Rev. A* **1985**, *31*, 1695−1697.

(42) Swope, W. C.; Andersen, H. C.; Berens, P. H.; Wilson, K. R. *J. Chem. Phys.* **1982**, *76*, 637−649.

(43) Plimpton, S. J. *J. Comput. Phys.* **1995**, *117*, 1−19.

(44) Plimpton, S. J.; Pollock, R.; Stevens, M. In *The Eighth SIAM Conference on Parallel Processing for Scientific Computing*: Minneapolis, 1997.

(45) Kirkwood, J. G.; Buff, F. P. *J. Chem. Phys.* **1949**, *17*, 338−343.

(46) Jasper, J. J. *J. Phys. Chem. Ref. Data* **1972**, *1*, 841−1009.

(47) Tsierkezos, N. G.; Molinou, I. E. *J. Chem. Eng. Data* **1998**, *43*, 989−993.

(48) Alvarez, E.; Rendo, R.; Sanjurjo, B.; Sanchez-Vilas, M.; Navaza, J. M. *J. Chem. Eng. Data* **1998**, *43*, 1027−1029.

(49) Zeppieri, S.; Rodriguez, J.; de Ramos, A. L. L. *J. Chem. Eng. Data* **2001**, *46*, 1086−1088.

(50) Yoshida, T.; Taga, K.; Okabayashi, H.; Matsushita, K.; Kamaya, H.; Ueda, I. *J. Colloid Interface Sci.* **1986**, *109*, 336−340.

(51) Kalinin, V. V.; Radke, C. J. *Colloids Surf., A* **1996**, *114*, 337−350.

(52) Soper, A. K.; Phillips, M. G. *Chem. Phys.* **1986**, *107*, 47−60.

(53) Clementi, E.; Barsotti, R. *Chem. Phys. Lett.* **1978**, *59*, 21−25.

(54) Mezei, M.; Beveridge, D. L. *J. Chem. Phys.* **1981**, *74*, 6902−6910.

(55) Chandrasekhar, J.; Spellmeyer, D. C.; Jorgensen, W. L. *J. Am. Chem. Soc.* **1984**, *106*, 903−910.

(56) Cieplak, P.; Kollman, P. *J. Chem. Phys.* **1990**, *92*, 6761−6767.

(57) Ferlat, G.; San Miguel, A.; Jal, J. F.; Soetens, J. C.; Bopp, P. A.; Daniel, I.; Guillot, S.; Hazeman, J. L.; Argoud, R. *Phys. Rev. B* **2001**, *6313*.

(58) Derjaguin, B. V.; Churaev, N. V. *J. Colloid Interface Sci.* **1978**, *66*, 389−398.

(59) Wantke, K. D.; Fruhner, H.; Fang, J. P.; Lunkenheimer, K. *J. Colloid Interface Sci.* **1998**, *208*, 34−48.

(60) Monroy, F.; Kahn, J. G.; Langevin, D. *Colloids Surf., A* **1998**, *143*, 251−260.

(61) Bergeron, V.; Waltermo, A.; Claesson, P. M. *Langmuir* **1996**, *12*, 1336−1342.

(62) Fruhner, H.; Wantke, K. D.; Lunkenheimer, K. *Colloids Surf., A* **2000**, *162*, 193−202.

(63) Langevin, D. *Adv. Colloid Interface Sci.* **2000**, *88*, 209−222.

(64) Persson, C. M.; Claesson, P. M.; Lunkenheimer, K. *J. Colloid Interface Sci.* **2002**, *251*, 182−192.

(65) Rusanov, A. I.; Krotov, V. V.; Nekrasov, A. G. *Colloid J.* **2004**, *66*, 339−342.

(66) Rusanov, A. I.; Krotov, V. V. *Colloid J.* **2004**, *66*, 204−207.

(67) Jang, S. S.; Jo, W. H. *J. Chem. Phys.* **1999**, *110*, 7524−7532.

(68) Jang, S. S.; Jo, W. H. *Macromol. Theory Simul.* **1999**, *8*, 1−9.

(69) Jang, S. S.; Jo, W. H. *Polymer* **1999**, *40*, 919−925.

(70) Nilsson, G. *J. Phys. Chem.* **1957**, *61*, 1135−1142.

(71) Matijevic, E.; Pethica, B. A. *Trans. Faraday Soc.* **1958**, *54*, 1382−1389.

(72) Clark, D. C.; Dann, R.; Mackie, A. R.; Mingins, J.; Pinder, A. C.; Purdy, P. W.; Russell, E. J.; Smith, L. J.; Wilson, D. R. *J. Colloid Interface Sci.* **1990**, *138*, 195−206.

(73) Lu, J. R.; Simister, E. A.; Lee, E. M.; Thomas, R. K. *Langmuir* **1992**, *8*, 1837−1844.

(74) Aronson, A. S.; Bergeron, V.; Fagan, M. E.; Radke, C. J. *Colloids Surf., A* **1994**, *83*, 109−120.

(75) Lu, J. R.; Hromadova, M.; Simister, E. A.; Thomas, R. K.; Penfold, J. *J. Phys. Chem.* **1994**, *98*, 11519−11526.

(76) Bergeron, V. *Langmuir* **1997**, *13*, 3474−3482.